Equiphase-sphere approximation for analysis of light scattering by arbitrarily shaped nonspherical particles

Xu Li, Zhigang Chen, Allen Taflove, and Vadim Backman

We extend the previously proposed concept of equiphase sphere (EPS) to analyze light-scattering properties of arbitrarily shaped particles. Our analyses based on the Wentzel–Kramers–Brillouin technique and numerical studies based on the finite-difference time-domain method demonstrate that a wide range of irregularly shaped particles can be approximated as their equivalent equiphase ellipsoids to determine their total scattering cross-section (TSCS) spectra. As a result, a simple expression given by the EPS approximation can be used to calculate the TSCS spectra of these particles. We find that the accuracy of the EPS approximation is influenced by both the magnitude and the geometric scale of the surface perturbation of the particle, and we derive validity conditions of the EPS approximation to guide the practical application of this method.

OCIS codes: 290.5850, 290.0290.

1. Introduction

Light scattering by nonspherical particles is of significant research interest in a variety of disciplines such as optical tissue diagnosis,[1–6] astronomy, meteorology, and remote sensing.[7] It is well known that most natural particles have nonspherical geometries. However, no general analytical theory has been developed to characterize light-scattering properties of arbitrarily shaped particles. These particles are often replaced by spheres with an equivalent volume, an equivalent surface area, or an equivalent cross-sectional area and then modeled with Mie theory. However, to our knowledge no systematic analysis has been developed to guide the optimum choice of the equivalent sphere of an arbitrary particle. Moreover, no general rules have been established to determine the validity criteria to apply such approximations. As a result, Mie theory has been applied in many applications only semiempirically at best. Therefore it is of critical importance to develop simple, yet accurate, approximation methods to model light scattering by a wide range of nonspherical particles and, importantly, identify their validity conditions.

Significant research interest has been focused on the spectral properties of the total scattering cross section (TSCS) of particles with sizes in the resonance range. TSCS plays a fundamental role not only in light scattering but also in light transport in turbid media. The most distinctive feature observed from the TSCS spectrum $\sigma_s(\lambda)$ of a spherical particle with refractive index $n < 3$ is the interference structure,[8] which refers to slow oscillations of the TSCS as a function of wavelength with the frequency of these oscillations proportional to the diameter of the particle. The interference structure is evidently noted in the well-known approximation derived by van de Hulst[9] for spherical particles with a low refractive index, i.e., n approaching 1.

$$\sigma_s(\lambda) = \frac{1}{2}\,\pi d^2[1 - 2\,\sin\rho/\rho + 4\,\sin^2(\rho/2)/\rho^2], \quad (1)$$

where d is the diameter of the spherical particle and ρ is the maximum phase shift of a light ray propagating through the particle along a straight path with respect to the phase shift of a light ray propagating outside the particle:

$$\rho = \frac{2\pi}{\lambda}\,d(n - 1). \quad (2)$$

All the authors are with Northwestern University, Evanston, Illinois 60208. X. Li (xuli@northwestern.edu) and V. Backman are with the Department of Biomedical Engineering. Z. Chen and A. Taflove are with the Department of Electrical and Computer Engineering.

Received 26 March 2004; revised manuscript received 18 May 2004; accepted 21 May 2004.

0003-6935/04/234497-09$15.00/0

With sufficiently large ρ, the higher-order term 4 $\sin^2(\rho/2)/\rho^2$ can be neglected in Eq. (1), and the oscillation of the interference structure is predominately due to the $\sin(\rho)/\rho$ term. Thus the diameter of the particle can be easily derived from the oscillation frequency:

$$d = \frac{1}{n-1}\frac{\lambda_1\lambda_2}{(\lambda_2-\lambda_1)}, \tag{3}$$

where λ_1 and λ_2 are wavelengths corresponding to two adjacent maxima or minima in the TSCS spectrum.

This direct association between the size of a spherical particle and the oscillation feature of its TSCS spectrum makes the van de Hulst approximation one of the most useful formulas in the domain of Mie theory. For applications involving nonspherical particles, however, it is important to answer the following questions: Is the interference structure a unique phenomenon for light scattering by spheres or it is preserved for nonspherical particles as well? If the latter case is true, how does the oscillation feature associate with the size and shape parameter of the particle? In other words, is it possible to derive approximations that explicitly link the particle size and shape parameters to its interference structure and to model light scattering by nonspherical particles? Furthermore, how do the shape characteristics of the particle affect the validity and accuracy of the approximation?

Motivated by the need to answer the above important questions, we previously introduced the concept of the equiphase sphere (EPS) to approximate the light-scattering characteristics of nonspherical particles.[10] We demonstrated both theoretically and numerically that certain spheroids exhibit interference structures in the TSCS spectra similar to those of spheres that generate equivalent maximum phase shifts. TSCSs of such spheroids can be modeled with the EPS approximation. We also provided the range of aspect ratios for which the EPS approximation is valid for spheroids. In our most recent study,[11] we conducted initial numerical experiments to test the feasibility of using the EPS approximation to calculate the TSCS spectra of a wide range of nonspherical shapes.

This paper is focused on the practical applicability of EPS approximation for arbitrarily shaped particles. We provide a detailed procedure to apply the EPS approximation to calculate the TSCS spectrum of an arbitrarily shaped particle (Section 2). We also present a theoretical analysis to determine the validity conditions on the particle-shape statistics under which the EPS approximation can be applied (Section 2). Finally, we report a comprehensive numerical study using finite-difference time-domain (FDTD) simulations[12] conducted on a wide range of particle shapes that supports our theoretical analyses (Section 3).

Throughout this paper, without loss of generality, the incident light is assumed to propagate in the $+\hat{z}$ direction. The expression $\sigma_s(\lambda)$ denotes the TSCS spectrum. The term $\sigma(f)$ without the subscript represents the standard deviation of the variable f. Finally, the symbol $\langle f \rangle$ denotes the mean of f.

2. Formulation and Validity of the Equiphase-Sphere Approximation

The geometric characteristics of an arbitrary nonspherical particle can be classified into two categories: the overall shape deviation from a sphere and the surface perturbation at smaller scales. The first property can be characterized by the aspect ratio of a best-fitting ellipsoid of the particle. The second property can be quantified with statistical parameters such as a radial standard deviation and the correlation length or correlation angle of the surface perturbation. The effect of each of these geometric properties on the TSCS spectrum of a nonspherical particle is investigated separately in Subsections 2.A and 2.B. The theoretical results presented are validated in our rigorous numerical experiments as discussed in Section 3.

A. Equiphase-Sphere Approximation for Spheroids and Ellipsoids

The natural extensions of a spherical shape include spheroids and ellipsoids. A spheroid is obtained when an ellipse is rotated about one of its principal axes; therefore it has two principal axes equal in length ($2a > 2b = 2c$ or $2a = 2b > 2c$). Ellipsoids are generalizations of spheroids with generally unequal principal axes ($2a \geq 2b \geq 2c$).

We first summarize the EPS approximation previously derived for spheroids.[10] To improve accuracy, the TSCS spectrum is given by the sum of the edge-effect term $\sigma_s^{(s)}$ and volume-diffraction-effect term $\sigma_s^{(v)}$:

$$\sigma_s(\lambda) = \sigma_s^{(s)}(\lambda) + \sigma_s^{(v)}(\lambda). \tag{4}$$

We note that the high-frequency ripple structure in the edge term $\sigma_s^{(s)}$ usually is not observed in experimental measurements of polydisperse particle ensembles. Therefore we neglect this effect. Thus $\sigma_s^{(s)}$ can be approximated as[10,11,13,14]

$$\sigma_s^{(s)}(\lambda) \approx 2S[2\pi(3V/4\pi)^{1/3}/\lambda]^{-2/3}, \tag{5}$$

where S is the particle's maximum cross-sectional area transverse to the direction of the incident light and V is the volume of the particle. The volume term $\sigma_s^{(v)}$ can be derived with the Wentzel–Kramers–Brillouin technique[11,15,16]:

$$\sigma_s^{(v)} = 2\ \mathrm{Re}\left(\iint_S \{1 - \exp[i\xi(\mathbf{r})]\} d^2\mathbf{r}\right), \tag{6}$$

where $\mathbf{r}$ is a position vector in the plane S and $\xi(\mathbf{r})$ is the phase shift of a light ray crossing plane S in point

r. By examining the light path-length distribution inside of a spheroidal particle, we derive $\sigma_s^{(v)}$ from the integration in Eq. (6), which is given by[10,14]

$$\sigma_s^{(v)}(\lambda) = 2S[1 - 2n \sin \rho/\rho + 4n \sin^2(\rho/2)/\rho^2], \quad (7)$$

where ρ is the maximum phase shift produced by a corresponding equiphase sphere that generates the same maximum phase shift as the spheroid. The diameter of the equiphase sphere d is equal to either the major axis $2a$ or minor axis $2b$ of the spheroid, depending on which axis aligns with the incident light.

In our previous study[10] we also derived the validity range of the equiphase sphere approximation to prolate ($a > b = c$) spheroids. We demonstrated both analytically and numerically that the oscillatory behavior of the TSCS spectrum of a spheroid follows that of its EPS in phase provided that

$$\rho \gg 1, \; n < 2, \quad (8)$$

$$\rho[\delta L(\mathbf{r})]_{\max} < \pi/2, \quad (9)$$

where $\delta L(\mathbf{r})$ is the path-length difference of light propagation inside a spheroid compared with that inside a sphere. For a spheroid with major axis $2a$ perpendicular to the incident light, inequality (9) is equivalent to

$$\beta \equiv 4(n-1)b\delta L/\lambda \approx \frac{16}{\pi^2}\frac{(n-1)^2}{n}\left(\frac{2a}{\lambda}\right)\left(\frac{b/a - b^2/a^2}{1 + a^2/b^2}\right) < 1. \quad (10a)$$

If the spheroid is oriented parallel to the incident light, inequality (9) becomes

$$\beta \equiv 4(n-1)a\delta L/\lambda \approx \frac{16}{\pi^2}\frac{(n-1)^2}{n}\left(\frac{2a}{\lambda}\right)\left(\frac{a/b - 1}{1 + b^2/a^2}\right) < 1. \quad (10b)$$

We note that for refractive index $n < 2$ and size range $2a \leq 10\lambda$, Eq. (10a) is satisfied for any aspect ratio a/b, whereas Eq. (10b) is satisfied only for a limited range of $a/b < (a/b)_{\max}$. For example, in the case in which $n = 1.5$ and $a = 10\lambda$, $(a/b)_{\max} \approx 1.4$ is the upper limit of the aspect ratio for Eq. (10b) to be satisfied. For a smaller refractive index $n = 1.1$, Eq. (10b) can be satisfied for much more elongated spheroids with aspect ratios as large as $(a/b)_{\max} \approx 5$.

The next step is to extend this analysis from spheroidal particles to ellipsoidal particles with one of the three axes parallel to the incident light. Without loss of generality, we assume that the semiaxis c is parallel to the incident light propagation direction $\hat{z}$ and semiaxis a and b are located in the transverse plane. Following the derivation presented in our previous study,[10] the volume term of the TSCS spectrum of an ellipsoid can also be approximated by Eq. (7) with

$$S = \pi ab, \quad (11)$$

$$\rho = \frac{4\pi}{\lambda} c(n-1). \quad (12)$$

The validity condition analogous to Eqs. (10a) and (10b) is given by

$$\beta \equiv 4(n-1)b\delta L/\lambda \approx \frac{16}{\pi^2}\frac{(n-1)^2}{n}\left(\frac{2c}{\lambda}\right)\left[\frac{|c/\min(a, b) - 1|}{1 + \min(a^2, b^2)/c^2}\right] < 1. \quad (13)$$

The criterion given in Eq. (13) can be intuitively interpreted as the following. Because Eq. (13) is derived from inequality (9), the intrinsic validity condition is that the path-length difference between the ellipsoid and its EPS δL must be small. Note that δL becomes greater as the direction of propagation of the light within the particle deviates from that of the incident light because of refraction. Therefore δL increases with higher refractive index [$\delta L \propto (n-1)^2/n$] and with increased curvature of the particle's front surface {$\delta L \propto |c/\min(a, b) - 1|/[1 + \min(a^2, b^2)/c^2]$}. Similar to the spheroidal particle cases, if the ellipsoid is oriented in the position such that the maximum cross-sectional plane is transverse to the incident light ($a > c$ and $b > c$), Eq. (13) is satisfied in most cases. Here the EPS approximation can be applied to calculate the TSCS spectrum of the ellipsoid as long as inequalities (8) are also satisfied.

For convenience of future discussion, we now reformulate the EPS approximation for ellipsoids by combining Eq. (4), approximation (5), and Eqs. (7) and (12). This yields

$$\sigma_s(\lambda) = 2S[2\pi(3V/4\pi)^{1/3}/\lambda]^{-2/3} + 2S[1 - 2n \sin \rho/\rho + 4n \sin^2(\rho/2)/\rho^2], \quad (14)$$

where $S = \pi ab$, $V = (4\pi)/(3)abc$, and $\rho = (4\pi)/(\lambda)c(n-1)$.

Note that the volume term in the EPS approximation [Eq. (7)] becomes equivalent to the van de Hulst approximation [Eq. (1)] for spheres with low refractive indexes, i.e., $n \to 1$ and $a = b = c$. However, the EPS approximation [Eq. (14)] includes an additional surface term $\sigma_s^{(s)}$. It also implicitly incorporates the effect of refraction, which is embedded in the derivation of Eq. (7). Therefore the EPS approximation provides improved accuracy even for spherical particles compared with the expression given by the van de Hulst approximation [Eq. (1)], particularly for higher refractive indices. More importantly, the EPS approximation predicts the interference structure in the TSCS spectra of ellipsoidal particles where the validity conditions of inequalities (8) and Eq. (13) are satisfied. The accuracy and validity condition of the EPS approximation applied to ellip-

soids are demonstrated with numerical studies presented in Subsection 3.A.

As evident from Eq. (14), the frequency of the TSCS spectrum oscillation is determined by the maximum longitudinal extent $2c$ of the ellipsoid, whereas the averaged magnitude of the TSCS is roughly proportional to the transverse cross-sectional area $S = \pi ab$. Therefore one can retrieve the size and aspect ratio of an ellipsoid from its TSCS spectrum in a straightforward manner.

B. Equiphase-Sphere Approximation for Arbitrarily Shaped Particles

To extend the EPS method to arbitrary shapes, we propose to approximate the TSCS spectrum of an irregularly shaped particle with the EPS-calculated TSCS of its best-fitting ellipsoid having one axis parallel to the incident light. If the validity criteria of inequalities (8) and Eq. (13) are satisfied for the best-fitting ellipsoid, the EPS approximation given by Eq. (14) can be used to calculate the TSCS spectrum of the irregularly shaped particle. In this subsection, we first define the best-fitting ellipsoid for an arbitrarily shaped particle and then discuss the effect of particle surface fluctuations on the validity of the approximation.

In general, finding the best-fitting ellipsoid for an arbitrary three-dimensional (3-D) shape is a multiparameter optimization problem with eight free parameters—three semiaxes (a, b, and c), three coordinates of the center (x_0, y_0, and z_0), and two rotational angles (θ_0 and ϕ_0). For our specific application, a few constraints can be added to simplify the optimization procedure. First, we specify one of the axes $2c$ to be aligned with the incident wave vector $\hat{z}$. Thus we have $\theta_0 = 0$. The second constraint is to match the cross-sectional area of the ellipsoid with the projected area of the particle in the $\hat{x}$–$\hat{y}$ plane ($S_p = \pi ab$). Furthermore, the location of the geometric center (x_0, y_0, z_0) is assigned to the center of mass of the irregular particle. Therefore we need to determine only three free parameters—the longitudinal semiaxis c, the aspect ratio of the cross section $\eta_T = a/b$, and the transverse rotational angle ϕ_0 (the angle between the cross-sectional major semiaxis a and $\hat{x}$). The objective of the optimization procedure is to minimize the mean-squared difference of the $\hat{z}$-directed light-ray path-length between the irregular particle and the corresponding ellipsoid. Parameters η_T, c, and ϕ_0 are chosen such that

$$\arg(c,\ \eta_T,\ \phi_0)|_{\min}(\langle\|\delta L_r\|^2\rangle). \tag{15}$$

The TSCS spectrum of the irregularly shaped particle is then approximated by that of its best-fitting ellipsoid, which can be calculated by Eq. (14).

The next step is to determine the influence of particle surface fluctuations on the validity of the EPS approximation. It is useful to statistically characterize these fluctuations to account for both the magnitude and the geometric scale. We use the root mean square (rms) of the path-length difference $R_{\delta L} \equiv (\langle\|\delta L\|^2\rangle)^{1/2}$ between the sample shape and its ellipsoidal counterpart to quantify the magnitude of the surface fluctuations and correlation angle Γ to parameterize the geometric scale of these fluctuations. Γ is defined as the solid angle within which the path-length difference δL is correlated.

The validity conditions of the EPS approximation for arbitrary particles are derived by examination of the Wentzel–Kramers–Brillouin integral given by Eq. (6). For a homogeneous irregularly shaped particle, the relative phase shift $\xi(\mathbf{r})$ inside the particle can be expanded as $\xi(\mathbf{r}) = \xi_0(\mathbf{r}) + \delta\xi(\mathbf{r})$, where $\xi_0(\mathbf{r}) = (2\pi)/(\lambda)(n - 1)L_0(\mathbf{r})$ is the phase shift in the best-fitting ellipsoid with path length $L_0(\mathbf{r})$, and the contribution due to the shape irregularity is given by $\delta\xi(\mathbf{r}) = (2\pi)/(\lambda)(n - 1)\delta L(\mathbf{r})$.

First, we stipulate that the average value of the phase shift is small:

$$\beta_1 \equiv \frac{2\pi}{\lambda}(n - 1)\langle\delta L(r)\rangle \ll 1. \tag{16}$$

This criterion is equivalent to one of the validity conditions of the Wentzel–Kramers–Brillouin approximation on which the EPS approximation is based: The wavelength of light cannot change significantly at a distance comparable to itself.[15]

Next, if

$$\left|\frac{1}{2\pi}\,\mathrm{Re}\int \exp(i\delta\xi)\mathrm{d}\varphi - 1\right| < 1,$$

$$\left|\frac{1}{2\pi}\int \exp(i\delta\xi)\mathrm{d}\varphi\right| < 1, \tag{17}$$

the exponent in Eq. (6) can be expanded to perform the integration analytically. This yields $\sigma_s^{(v)} \approx \sigma_{\mathrm{EPS}}^{(v)} + \delta\sigma^{(v)}$, and the EPS approximation is valid provided that $\delta\sigma^{(v)} \ll \sigma_{\mathrm{EPS}}^{(v)}$.

We assume that $\delta\xi$ is a stochastic function of $\mathbf{r}$. Inequalities (17) are satisfied if

$$\sigma\left(\frac{1}{2\pi}\int \delta\xi\mathrm{d}\varphi\right) < \frac{\pi}{2}. \tag{18}$$

Replacing the integral in inequality (18) by a summation, we obtain

$$\sigma\left(\frac{1}{2\pi}\int \delta\xi\mathrm{d}\varphi\right) \approx \frac{n-1}{\lambda}\,\sigma\left(\sum_{i=1}^{N}\delta L_i\delta\varphi_i\right)$$

$$\approx \frac{n-1}{\lambda}\,\delta\varphi\sigma[\delta L(\mathbf{r})]\sqrt{N}, \tag{19}$$

where $\delta\varphi$ is the angle within which δL is correlated. Thus $\delta\varphi = \Gamma$, $N = 2\pi/\Gamma$, and the second EPS validity criterion of inequality (18) becomes

$$\beta_2 \equiv \frac{2\sqrt{2}}{\lambda\sqrt{\pi}}(n - 1)\sqrt{\Gamma}\sigma[\delta L(\mathbf{r})] < 1. \tag{20}$$

To summarize the above analysis, to apply the EPS approximation to an arbitrarily shaped particle, the condition of Eq. (13) needs to be satisfied for its best-fitting ellipsoid. The conditions of Eqs. (16) and (20) provide additional validity criteria accounting for the surface fluctuations of the particle. Numerical studies validating the accuracy and validity conditions of the EPS approximation applied to irregularly shaped particles are presented in Subsection 3.C and 3.D.

3. Numerical Results

To verify the EPS approximation and its validity conditions derived in Section 2, we conducted numerical experiments for a wide range of particle shapes. Comparison of the TSCS spectra calculated with the EPS approximation with numerical FDTD benchmark data permit us to validate the EPS approximation and to explore the correlation between the approximation accuracy and the geometric characteristics of the particles. We first demonstrate the application of the EPS approximation to ellipsoids with a variety of aspect ratios. Subsequently, we demonstrate the effect of surface fluctuations of irregularly shaped particles on the accuracy of the EPS approximation using Gaussian random spheres, which are a class of well-parameterized geometries capable of representing natural and artificial shapes with varying deviations from spheres,[17] as geometric models.

A. Comparison of Total Scattering Cross-Sectional Spectra Calculated by the Finite-Difference Time-Domain Method and the Equiphase-Sphere Approximation for Ellipsoids

The FDTD method numerically solves the Maxwell's equations and thus provides exact solutions to many scattering problems. We use 3-D FDTD simulations to accurately characterize the light-scattering properties of a wide variety of geometries. We have extensively validated our FDTD code by computing the scattering patterns of homogeneous spheres and comparing the results with Mie theory. The geometry of a particle having its size scaled to the resonance range is imported to the FDTD grid by a staircasing scheme with 25-nm resolution. The FDTD grid is terminated by a Berenger perfectly matched layer absorbing boundary condition.[18] The total-field–scattered-field technique[19] is employed to source an $\hat{x}$-polarized plane wave propagating in the $+\hat{z}$ direction within the FDTD grid. We choose a modulated Gaussian pulse as the time-domain source waveform that accommodates the complete frequency range of visible light. The scattered-field frequency response is extracted by a discrete Fourier transform of the time-domain data recorded on the six surfaces of the scattered-field region and normalized by the spectrum of the source pulse. A 3-D near to far-field transformation in the phasor domain[20] is implemented to calculate the far-field scattered wave in the forward direction, and the TSCS spectrum is calculated with the extinction formula for nonabsorbing particles.[9]

FDTD simulations are conducted for ellipsoidal particles with a wide range of aspect ratios to validate the EPS approximation. Figure 1 shows six representative examples of our numerical experiments. In these examples, the lengths of two axes of the ellipsoids are fixed, i.e., $2c = 3.5$ μm, $2b = 3.0$ μm, whereas the length of the third axis $2a$ is varied from 4.5 to 1.5 μm in Figs. 1(a)–1(f) to yield varying aspect ratios. The refractive index of the particle is fixed at 1.5 in each case. The TSCS spectra are calculated from the FDTD simulations over the wavelength range of 500–1000 nm to serve as benchmark data. The EPS approximation of Eq. (14) is used to calculate the TSCS spectrum of each ellipsoidal particle and is compared with the FDTD data. The β factor in the validity condition of Eq. (13) is calculated for these particles. As illustrated in Figs. 1(a)–1(d), when the validity condition of Eq. (13) is satisfied, i.e., $\beta < 1$, the oscillatory interference structures in the TSCS spectra calculated by the EPS approximation are in phase with the benchmark data provided by the FDTD method. In the cases of Figs. 1(d) and 1(e) where $\beta > 1$, however, the oscillatory period of the TSCS spectrum of the particle completely departs from the one calculated by the EPS approximation. Therefore Fig. 1 demonstrates the significance of the validity condition of Eq. (13) to predict whether the EPS approximation can be applied to an ellipsoid with a certain aspect ratio.

B. Geometric Model for Irregularly Shaped Particles—Gaussian Random Spheres

To investigate the validity and accuracy of the EPS approximation applied to arbitrarily shaped particles, we use Gaussian random spheres as geometric models. We define a Gaussian random sphere in spherical coordinates as having the following angle-dependent radius:

$$r(\vartheta, \varphi) = \frac{R}{\sqrt{1 + \Delta^2}} \exp[s(\vartheta, \varphi)], \tag{21}$$

where R is the mean radius and Δ is the normalized standard deviation of the radius. $s(\vartheta, \varphi)$ is the log radius, which defines the shape of the particles. $s(\vartheta, \varphi)$ is given as a real-valued series expansion of spherical harmonics Y_{lm} with degree l and order m:

$$s(\vartheta, \varphi) = \sum_{l=0}^{\infty} \sum_{m=-l}^{l} s_{lm} Y_{lm}(\vartheta, \varphi). \tag{22}$$

The weights s_{lm} are selected on the basis of particle geometry statistics, which is determined by the covariance function $\Sigma_s = C_s(\delta\Omega)\ln(\Delta^2 + 1)$, the product of the correlation function C_s, and the log variance $\ln(\Delta^2 + 1)$ of the log radius. The log variance $\ln(\Delta^2 + 1)$ determines the amplitude of the variation of the radius. $C_s(\delta\Omega)$ describes the correlation of the radius $r(\vartheta, \varphi)$ over the angular displacement $\delta\Omega$. If the correlation function is constant [$C_s(\delta\Omega) = 1$], the resulting shape is a sphere. On the other hand, for irregular particles, $C_s(\delta\Omega)$ decreases with increasing angular displacement. A steep decline of $C_s(\delta\Omega)$

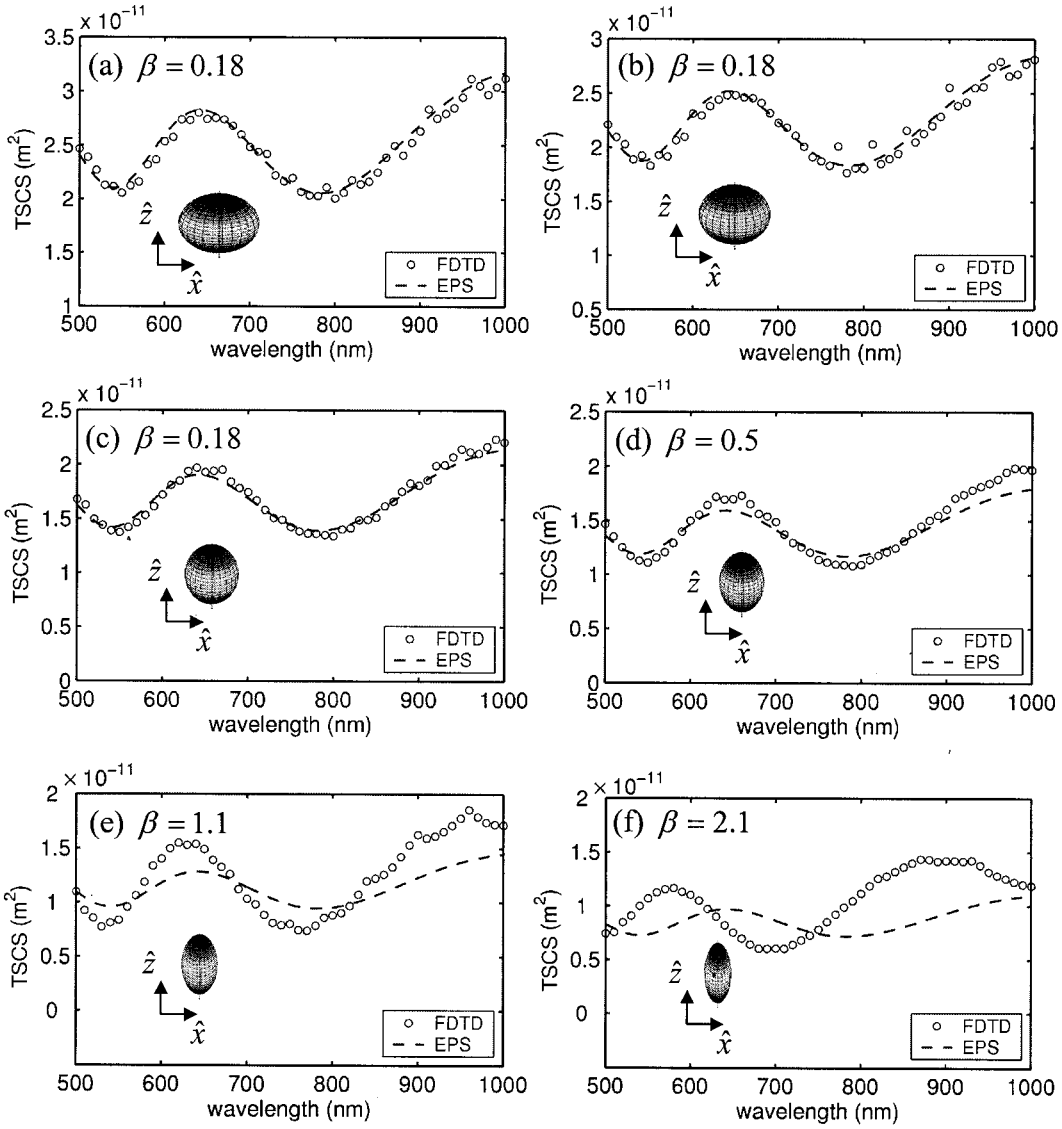

Fig. 1. TSCS spectra calculated with FDTD simulations and EPS approximations for ellipsoids with different aspect ratios. $\hat{z}$ is the wave vector of the incident light in the legends illustrating the geometry and orientation of the particles. (a) $2a = 4.5$ μm, $2b = 3.0$ μm, $2c = 3.5$ μm, $\beta = 0.18$; (b) $2a = 4.0$ μm, $2b = 3.0$ μm, $2c = 3.5$ μm, $\beta = 0.18$; (c) $2a = 3.5$ μm, $2b = 3.0$ μm, $2c = 3.5$ μm, $\beta = 0.18$; (d) $2a = 2.5$ μm, $2b = 3.0$ μm, $2c = 3.5$ μm, $\beta = 0.5$; (e) $2a = 2.0$ μm, $2b = 3.0$ μm, $2c = 3.5$ μm, $\beta = 1.1$; (f) $2a = 1.5$ μm, $2b = 3.0$ μm, $2c = 3.5$ μm, $\beta = 2.1$.

with $\delta\Omega$ results from small-scale perturbations of the particle shape. In this paper we use the modified Gaussian correlation function following the research of Muinonen *et al.*[21]:

$$C_s(\Omega) = \exp\left[-\frac{\sin^2(\Omega/2)}{2\sin^2(\gamma_g/2)}\right], \tag{23}$$

where γ_g is the correlation angle of the Gaussian sphere—the angular displacement over which the correlation drops to $1/\sqrt{e}$. Thus the geometry statistics of the particle are specified solely by Δ and γ_g.

We generate the 3-D geometry of Gaussian spheres in the spherical coordinates using a computer program based on the code developed by Muinonen and Nousiainen.[22] As shown in Figs. 2(a)–2(c), increasing Δ results in an increased magnitude of deformation from a sphere in the particle shape. On the other hand, as illustrated in Figs. 2(d)–2(f), reducing γ_g leads to an increased short-distance fluctuation (increased numbers of valleys and hills) on the particle surface.

C. Comparison of Total Scattering Cross-Sectional Spectra Calculated by the Finite-Difference Time-Domain Method and the Equiphase-Sphere Approximation for Gaussian Random Spheres

We conducted FDTD simulations for Gaussian spheres with Δ ranging from 0.1 to 0.9 and γ_g ranging from 10° to 90°. The geometries of the Gaussian spheres are converted to the Cartesian coordinates and incorporated into the FDTD grids with 25-nm

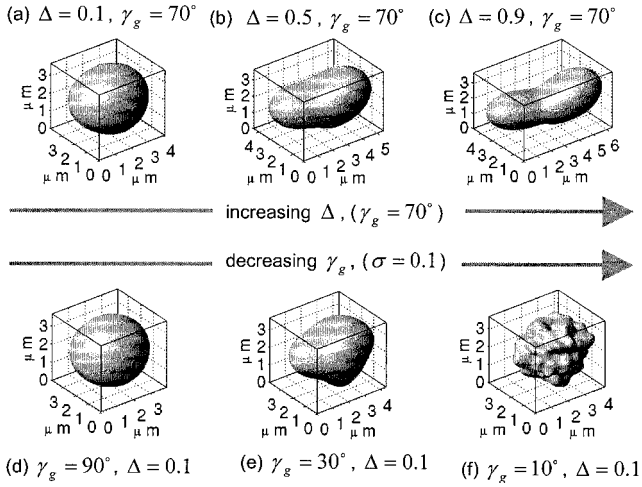

Fig. 2. Representative Gaussian sphere geometries. (a)–(c) Gaussian spheres with increasing Δ (γ_g is fixed at 70°). (d)–(f) Gaussian spheres with decreasing γ_g (Δ is fixed at 0.1).

resolutions. The particles are assigned a mean diameter of the order of 3.5 μm and a refractive index of 1.5. The EPS approximation given by Eq. (14) is applied to calculate the TSCS spectra of the particles after finding their best-fitting ellipsoids.

Figure 3 illustrates six examples of our numerical experiments conducted on a variety of Gaussian spheres. In each example, displayed from left to right, the geometry and size of the Gaussian sphere are illustrated in the first panel; the corresponding best-fitting ellipsoids are shown in the second panel; and the comparison of the spectra calculated by FDTD and the EPS approximation are plotted in the third panel. For the particles illustrated in the cases of Figs. 3(a)–3(c) we can see that the TSCS spectra calculated by the EPS approximation closely resemble the benchmark data provided by FDTD method. In the cases of Figs. 3(d) and 3(e) the TSCS spectra calculated with the EPS approximation start to deviate from the FDTD data. In the case of Fig. 3(f) the oscillatory period of the TSCS spectrum of the particle completely departs from that of its best-fitting ellipsoid, and the EPS approximation is not valid in the calculation of the TSCS spectrum for this case. As discussed in Subsection 3.D, both the excellent accuracy of the EPS approximation in the cases of Figs. 3(a)–3(c) as well as its relatively poor performance in the cases of Figs. 3(d)–3(f) can be explained with the validity analysis presented in Section 2.

D. Validity and Accuracy of the Equiphase-Sphere Approximation with Respect to Particle Surface Fluctuations

In a previous study[10] we investigated the correlation between the aspect ratio and the validity of the EPS approximation for spheroidal particles. There our numerical study supported the validity criteria given in Eqs. (10a) and (10b). The numerical experiments presented in Subsection 3.A also support the validity

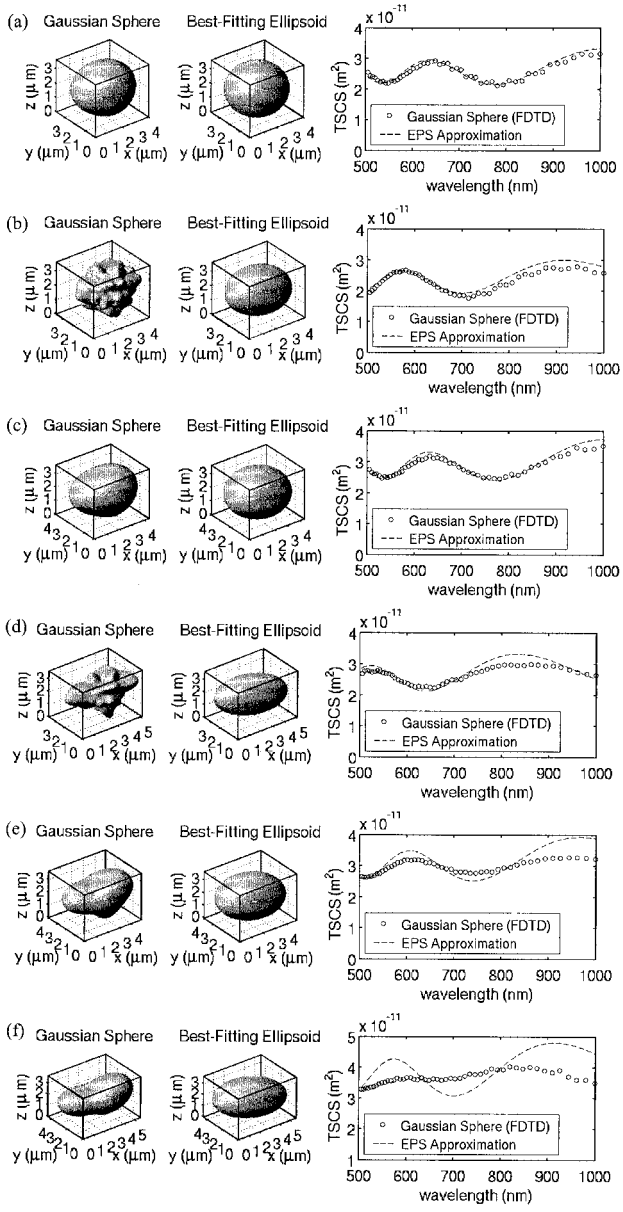

Fig. 3. TSCS spectra calculated by FDTD simulations and EPS approximations for a variety of Gaussian spheres. The geometries of the Gaussian sphere and its corresponding best-fitting ellipsoid are illustrated on the left two panels for each example. The incident light propagates in the $\hat{z}$ direction. (a) Δ = 0.1, γ_g = 70°; (b) Δ = 0.1, γ_g = 10°; (c) Δ = 0.2, γ_g = 70°; (d) Δ = 0.2, γ_g = 15°; (e) Δ = 0.2, γ_g = 40°; (f) Δ = 0.6, γ_g = 70°.

condition of Eq. (13) for ellipsoidal particles. In this subsection we focus on the effect of particle surface fluctuations on the accuracy of the EPS approximation.

The examples shown in Fig. 3 illustrate both the particle shapes for which the EPS approximation gives fairly accurate results and for which the approximation cannot be applied. To systematically investigate the validity and accuracy of the EPS method, we conducted a parametric study of the accuracy of the approximate TSCS spectra with respect to the FDTD benchmark data. Two complementary

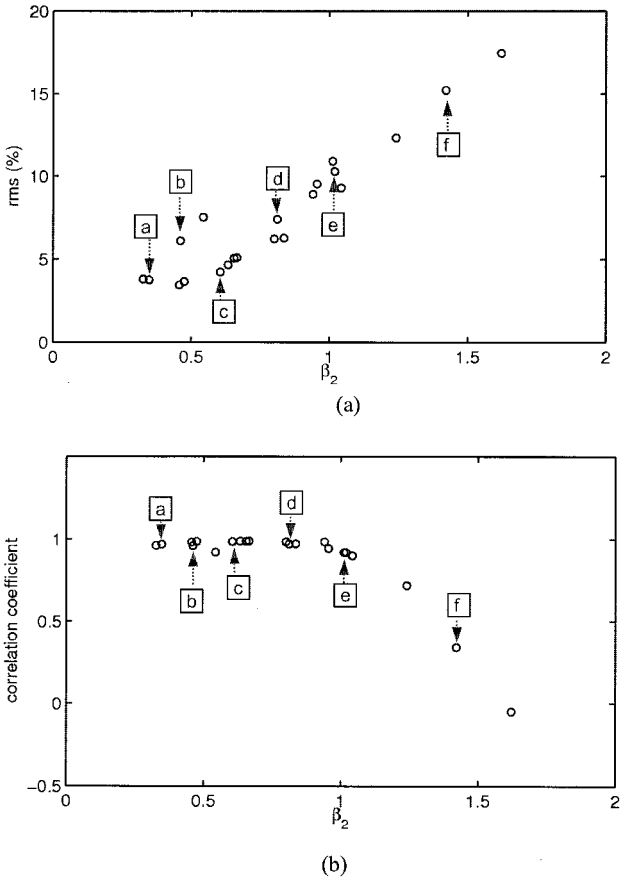

Fig. 4. Accuracy measurements of the EPS approximation as functions of the validity condition of parameter β_2. The labeled data points correspond to the cases illustrated in Figs. 3(a)–3(f). FDTD simulation results are used as the benchmark data. (a) rms error (%) versus β_2, (b) correlation coefficient versus β_2.

measures are considered: rms error R and the correlation coefficient r_c. The rms error measures the overall estimation accuracy whereas the correlation coefficient, which is evaluated with data recorded at N wavelengths λ_i,

$$r_c \equiv \frac{\sum_{i=1}^{N} \{[\mathrm{TSCS}_{\mathrm{FDTD}}(\lambda_i) - \langle \mathrm{TSCS}_{\mathrm{FDTD}}(\lambda)\rangle][\mathrm{TSCS}_{\mathrm{EPS}}(\lambda_i) - \langle \mathrm{TSCS}_{\mathrm{EPS}}(\lambda)\rangle]\}}{N\sigma[\mathrm{TSCS}_{\mathrm{FDTD}}(\lambda)]\sigma[\mathrm{TSCS}_{\mathrm{EPS}}(\lambda)]}, \tag{24}$$

quantifies the capability of the EPS approximation to replicate the frequency oscillation characteristics of the TSCS spectrum.

Note that all particles considered here have best-fitting ellipsoids that satisfy the validity criterion of Eq. (13). We further note that the validity condition of Eq. (16) is satisfied for most convex particles when the best-fitting ellipsoid is properly chosen. Thus the β_2 factor in the validity condition of Eq. (20) is the most important parameter that effects the accuracy and validity of the EPS approximation.

The influence of the β_2 factor on the validity of the EPS approximation is illustrated in Figs. 4(a) and 4(b), where we plot the percent rms error and the correlation coefficient as functions of β_2 for 23 Gaussian spheres covering a wide range of shapes (Δ ranging from 0.1 to 0.9 and γ_g ranging from 10° to 90°). To calculate β_2, λ_0 is chosen as the central wavelength of our range of interest (500–1000 nm), i.e., $\lambda_0 = 750$ nm. The surface fluctuation correlation angle Γ is approximated by γ_g, the correlation angle of the Gaussian sphere, because both angles quantify the angular scale within which a geometric feature is present. To better illustrate the connection between the quality of the EPS approximation and the accuracy measurements, we cross reference six data points in Figs. 4(a) and 4(b) with their corresponding particle geometries and the TSCS spectra shown in Figs. 3(a)–3(f).

We observe from Fig. 4 that when the criterion of Eq. (20) is satisfied ($\beta_2 < 1$), the EPS approximation is sufficiently accurate, i.e., the rms error $R < 10\%$ and the correlation coefficient $r_c \geq 0.9$. Figure 4(b) further reveals that when $\beta_2 > 1$, the accuracy of the EPS approximation degrades rapidly as β_2 increases. This further demonstrates the importance of the parameter β_2 in when we determine the validity of the EPS approximation.

We note from the validity criterion of Eq. (20) that β_2 is proportional to the square root of the correlation angle Γ when the magnitude of the surface fluctuation $\sigma[\delta L(r)]$ is fixed. The geometric interpretation is that surface perturbations within smaller angular scales have less effect on the validity of the EPS approximation. This provides the explanation for the two cases shown in Figs. 3(d) and 3(e), where the seemingly more irregular particle in Fig. 3(d) can be better treated by the EPS approximation than the apparently less irregular particle in Fig. 3(e).

4. Summary and Discussion

In this paper we have presented the EPS approximation to characterize light-scattering properties of arbitrarily shaped particles. Our analytical and numerical studies reveal that the interference structure characteristic of the TSCS spectrum of a spherical particle with a size in the resonance range is also present for a wide range of irregularly shaped particles. We also demonstrate that the TSCS spectra of irregularly shaped particles can be easily calculated by the EPS approximation. Because of its mathematical simplicity, the EPS approximation can be used to probe the size and geometric characteristics of a wide variety of irregularly shaped particles from their TSCS spectra. The vertical axis length $2c$ of the best-fitting ellipsoid of a particle, which is an estimation of the longitudinal extent of the particle, can be easily

derived from the periodicity of the interference structure by use of Eq. (3).

Furthermore, we have derived and verified the validity criteria of the EPS approximation to guide the practical application of this method. The validity analysis should enable researchers to determine when this approximation can and, importantly, cannot be used to model light interaction with nonspherical particles based on the particle geometry.

Overall, we have demonstrated that the effective, yet easy to use, EPS approximation can be used to model light scattering by a wide range of nonspherical particles when certain validity criteria are satisfied. This method may become a valuable tool for the analysis of light scattering by random particles in many applications.

We acknowledge the financial support by the National Science Foundation under grants BES-0238903 and ACI-0219925. We also express our gratitude to the authors of the original Gaussian random sphere generation code, K. Muinonen and T. Nousiainen, for making their code publicly available.

References

1. L. T. Perelman, V. Backman, M. Wallace, G. Zonios, R. Manoharan, A. Nusrat, S. Shields, M. Seiler, C. Lima, T. Hamano, I. Itzkan, J. V. Dam, J. M. Crawford, and M. S. Feld, "Observation of periodic fine structure in reflectance from biological tissue: a new technique for measuring nuclear size distribution," Phys. Rev. Lett. **80,** 627–630 (1998).
2. J. R. Mourant, T. M. Johnson, S. Carpenter, A. Guerra, T. Aida, and J. P. Freyer, "Polarized angular dependent spectroscopy of epithelial cells and epithelial cell nuclei to determine the size scale of scattering structures," J. Biomed. Opt. **7,** 378–387 (2002).
3. A. Wax, C. Yang, M. Müller, R. Nines, C. W. Boone, V. E. Steele, G. D. Stoner, R. R. Dasari, and M. S. Feld, "*In situ* detection of neoplastic transformation and chemopreventive effects in rat esophagus epithelium using angle-resolved low-coherence interferometry," Cancer Res. **63,** 3556–3559 (2003).
4. Y. L. Kim, Y. Liu, R. K. Wali, H. K. Roy, M. J. Goldberg, A. K. Kromine, K. Chen, and V. Backman, "Simultaneous measurement of angular and spectral properties of light scattering for characterization of tissue microarchitecture and its alteration in early precancer," IEEE J. Sel. Top. Quantum Electron. **9,** 243–256 (2003).
5. H. K. Roy, Y. Liu, R. Wali, Y. L. Kim, A. K. Kromine, M. J. Goldberg, and V. Backman, "Four-dimensional elastic light-scattering fingerprints as preneoplastic markers in the rat model of colon carcinogenesis," Gastroenterology **126,** 1071–1081 (2004).
6. J. W. Pyhtila, R. N. Graf, and A. Wax, "Determining nuclear morphology using an improved angle-resolved low coherence interferometry system," Opt. Exp. **11,** 3473–3484 (2003), http://www.opticsexpress.org.
7. M. I. Mishchenko, J. W. Hovenier, and L. D. Travis, *Light Scattering by Nonspherical Particles: Theory, Measurements and Applications* (Academic, San Diego, Calif., 2000).
8. P. Chylek and J. Zhan, "Interference structure of the Mie extinction cross section," J. Opt. Soc. Am. A **6,** 1846–1851 (1989).
9. H. C. van de Hulst, *Light Scattering by Small Particles* (Dover, New York, 1981).
10. Z. Chen, A. Taflove, and V. Backman, "Concept of the equiphase sphere for light scattering by nonspherical dielectric particles," J. Opt. Soc. Am. A **21,** 88–97 (2004).
11. X. Li, Z. Chen, J. Gong, A. Taflove, and V. Backman, "Novel analytical techniques to address forward and inverse problems of light scattering by irregularly shaped particles," Opt. Lett. **29,** 1239–1401 (2004).
12. A. Taflove and S. Hagness, *Computational Electrodynamics: The Finite-Difference Time-Domain Method* (Artech House, Boston, Mass., 2000).
13. H. Nussenzveig and W. Wiscombe, "Efficiency factors in Mie scattering," Phys. Rev. Lett. **45,** 1490–1494 (1980).
14. Z. Chen, A. Taflove, and V. Backman, "Equivalent volume-averaged light scattering behavior of randomly inhomogeneous dielectric spheres in the resonant range," Opt. Lett. **28,** 765–767 (2003).
15. C. M. Bender and S. A. Orszag, *Advanced Mathematical Methods for Scientists and Engineers: Asymptotic Methods and Perturbation Theory* (Springer-Verlag, New York, 1999).
16. J. D. Klett and R. A. Sutherland, "Approximate methods for modeling the scattering properties of non-spherical particles: evaluation of the Wentzel–Kramers–Brillouin method," Appl. Opt. **31,** 373–386 (1992).
17. K. Muinonen, "Light scattering by stochastically shaped particles," in *Light Scattering by Nonspherical Particles: Theory, Measurements, and Applications*, M. I. Mishchenko, J. W. Hovenier, and L. D. Travis, eds. (Academic, San Diego, Calif., 2000).
18. J. P. Berenger, "A perfectly matched layer for the absorption of electromagnetic waves," J. Comput. Phys. **114,** 185–200 (1994).
19. K. R. Umashankar and A. Taflove, "A novel method to analyze electromagnetic scattering of complex objects," IEEE Trans. Electromagn. Compat. **24,** 397–405 (1982).
20. A. Taflove and K. R. Umashankar, "Radar cross-section of general three-dimensional structures," IEEE Trans. Electromagn. Compat. **25,** 433–440 (1983).
21. K. Muinonen, T. Nousiainen, P. Fast, K. Lumme, and J. I. Peltoniemi, "Light scattering by Gaussian random particles: ray optics approximation," J. Quant. Spectrosc. Radiat. Transfer **55,** 577–601 (1996).
22. K. Muinonen and T. Nousiainen, G-sphere, 2002. Available under the GNU General Public License, http://www.meteo.helsinki.fi/~tpnousia/gsphere/index.html.